JOURNAL OF SOLID STATE CHEMISTRY **121,** 437–442 (1996)
ARTICLE NO. 0060

Structure, Dielectric Properties, and Thermal Expansion of the New Phase $Hf_{0.75}Sn_{0.25}O_2$

R. Mackay and A. W. Sleight

Department of Chemistry, Oregon State University, Corvallis, Oregon 97331-4003

and

M. A. Subramanian

Central Research and Development Department, E. I. duPont de Nemours & Co., Wilmington, Delaware 19880-0328

Received July 10, 1995; in revised form October 9, 1995; accepted October 25, 1995

A new phase with the α-PbO_2 structure has been discovered with the composition $Hf_{0.75}Sn_{0.25}O_2$. Single crystals were prepared in a potassium borate flux. The structure was refined from single crystal X-ray diffraction data, leading to $R = 0.026$. The space group is *Pbcn* with $a = 4.86(1)$, $b = 5.699(1)$, and $c = 5.204(1)$ Å. Over the temperature range from 30 to 800°C, a rather low thermal expansion ($\sim 4 \times 10^{-6}$/°C) is observed. The dielectric constant of a $Hf_{0.75}Sn_{0.25}O_2$ sample measured from 10^3 to 10^7 Hz and from room temperature to 300°C was found to be 13; the dielectric loss is very low.

INTRODUCTION

Certain compositions having the α-PbO_2 structure are found to have excellent properties for dielectric resonators operating at microwave frequencies (1–8). For example, the composition $Zr_{0.4}Sn_{0.1}Ti_{0.5}O_2$ has a moderate dielectric constant (~38), a low dielectric loss ($Q \sim 7000$ at 7 Ghz), and a temperature coefficient of resonant frequency less than 1 ppm/°C (2). These values are sensitive to composition variations and processing conditions.

The α-PbO_2 structure is similar to the rutile structure in that it can be regarded as based on hexagonal close-packed oxygen layers with cations occupying half of the octahedral sites. The filling pattern of the octahedral sites is, however, different in the two structures. In the rutile structure, a linear chain of edge-shared octahedra results, whereas in the α-PbO_2 structure, a zigzag chain of edge-shared octahedra results. Metal–metal bonding across the shared edge can favor the α-PbO_2 structure in the d^3 situation such as pertains to ReO_2 (9). However, d electron concentration cannot be used to explain the occurrence of the α-PbO_2 structure for PbO_2 or compositions in the ZrO_2–TiO_2, HfO_2–TiO_2, ZrO_2–SnO_2, and ZrO_2–SnO_2–TiO_2 systems. Apparently, the α-PbO_2 structure also becomes competitive with the rutile structure for larger cations. This point was made by Muller and Roy for $M^{3+}M^{5+}O_2$ compounds (10). The average size of the cation in the ZrO_2- or HfO_2-based compositions with the α-PbO_2 structure may also be considered large relative to the usual cation size in the rutile structure. Several compounds with the rutile structure, including SnO_2 and TiO_2, transform at high pressure to the α-PbO_2 structure with a 1–2% increase in density (10).

The α-PbO_2 structure exists for ZrO_2–TiO_2, HfO_2–TiO_2, ZrO_2–SnO_2, and ZrO_2–TiO_2–SnO_2 solid solutions (1–8, 11) but does not exist for any of these end members under ordinary conditions. In the case of the ZrO_2–SnO_2 system, compositions with the α-PbO_2 structure are apparently metastable at one atmosphere and room temperature (1). Cation ordering in these compositions is not usually observed. However, annealing the composition $5ZrO_2 \cdot 7TiO_2$ does result in cation ordering and a tripled a axis (13).

The thermal expansion of ZrO_2- and HfO_2-based compositions with the α-PbO_2 structure has been of some interest (14–17). Low thermal expansion is found for compositions in the HfO_2–TiO_2 systems. The behavior is typical of low-thermal-expansion anisotropic materials (18) such as cordierite; that is, expansion in some directions is compensated for by contraction in others. The net result is very low volume expansion. In the case of HfO_2–TiO_2 compositions with the α-PbO_2 structure, while the a and c axes expand with increasing temperature, the b axis contracts. The α-PbO_2 structure exists over a considerable range of composition in the HfO_2–TiO_2 system, and the thermal expansion behavior is highly sensitive to the Hf/Ti ratio (15). For ZrO_2–TiO_2 compositions with the α-PbO_2 structure, there is expansion along all three axes with

0022-4596/96 $18.00

TABLE 1
Crystal Data for $Hf_{0.75}Sn_{0.25}O_2$

Formula	$Hf_{0.77}Sn_{0.23}O_2$
Space Group	*Pbcn* (No. 60)
a, Å	4.861(1)
b, Å	5.699(1)
c, Å	5.204(1)
V, Å^3	144.2(7)
d_{calc}, g/cm^3	9.10
Crystal size, mm^3	0.16 × 0.06 × 0.02
μ(Mo$K\alpha$), cm^3	594.3
Data collection instrument	Rigaku AFC6R
Radiation (monochromated in incident beam)	Mo$K\alpha$ (λ = 0.71069 Å)
Temperature, °C	23
Scan method	$\omega - 2\theta$
Octants measured	$-h \rightarrow h$, $0 \rightarrow k$, $0 \rightarrow l$
Data collection range, 2θ	0–65
No. reflections measured	605
No. unique data, total with $F_o^2 > 3\sigma(F_o^2)$	181
No. parameters refined	17
Transmission factors, max/min	1.736
Secondary extinction coefficient	$9.4(4) \times 10^{-6}$
R^a, Rw,^{b} GOF^c	0.026, 0.030, 1.099
Largest difference peak, e/Å^3	2.97
Largest neg. difference peak, e/Å^3	−3.00

[a] $R = \Sigma| |F_o| - |F_c| |/\Sigma | F_o|$.
[b] $R_w = [\Sigma(|F_o| - |F_c|)^2/\Sigma w | F_o|^2]^{1/2}$; $w = 1/\sigma^2(|F_o|)$.
[c] GOF = $(\Sigma(|F_o| - |F_c|)/\sigma i)/(N_{obs.\ refl.} - N_{parameters})$.

increasing temperature. However, addition of SnO_2 to the ZrO_2–TiO_2 system lowers the thermal expansion. Thus for the composition $Zr_{0.5}Sn_{0.3}Ti_{0.2}O_4$, the thermal expansion is nearly as low as it is for HfO_2–TiO_2 compositions. Addition of SnO_2 to the HfO_2–TiO_2 compositions has very little effect on thermal expansion. The composition with the α-PbO_2 structure reported to have the lowest thermal expansion for this structure type is $Hf_{0.25}Zr_{0.25}Sn_{0.25}Ti_{0.25}O_2$.

The phase diagram for the ZrO_2-TiO_2-SnO_2 system is reported (1). However, despite the interest in the dielectric and thermal expansion properties of compounds with the α-PbO_2 structure, there has apparently been no previous investigation of the simple HfO_2–SnO_2 system.

EXPERIMENTAL

Synthesis. Single crystals suitable for X-ray diffraction were prepared by combining the powders HfO_2 (Teledyne Wah Chang), SnO_2 (Baker Analytical, 99%), and KNO_3 (EM Science, 99.97%), with B_2O_3 (ÆSAR, 99%) in a molar ratio 1:1:4:10. The mixture was heated in a Pt crucible at 1400°C for 12 hours, evaporating the flux to dryness. The resulting two-phase mixture had a pinkish hue and contained transparent needle- and plate-like crystals. A single-phase powder sample was prepared by combining HfO_2 and SnO_2 in the molar ratio 7:3 with excess B_2O_3 and heating at 1400°C for 8 hours. A sol–gel method was also used to prepare a single-phase sample by following the procedure of Kudesia *et al.* (6), using $HfOCl_2 \cdot 8H_2O$. The sample for dilatometry measurements was made by heating a mixture of HfO_2 and SnO_2 in the mole ratio 3:1 in a covered crucible at 1050°C for 2 hours. The sample was reground and, with 2 drops of a 5% polyvinyl alcohol (PVA) solution added as binder, pressed into a pellet. It was heated again in a covered crucible at 1350°C for 4 hours. The final dimensions of the pellet was 26.2 × 5.1 × 3.9 mm. A sample of $HfTiO_4$ was prepared for thermal expansion measurements by heating an equimolar mixture of HfO_2 and TiO_2 (Baker Analytical) at 1450°C for 8 hours and at 1550°C for 6 hours, with grinding between heatings. PVA was added as a binder before pressing a pellet, which was again heated to 1550°C and held for 6 hours. The final dimensions were 24.5 × 4.7 × 4.2 mm.

Characterization. X-ray diffraction data on powders were collected on a Siemens D5000 diffractometer. Lattice parameters were determined by a least-squares fit on the data using an internal Si reference standard. Single-crystal diffraction data were collected on a Rigaku AFC6R diffractometer. Instrument parameters are listed

TABLE 2
Positional Parameters for $Hf_{0.75}Sn_{0.25}O_2$

Atom	*x*	*y*	*z*	*B*(eq)	Occupancy
Hf	0.0	0.17811(6)	1/4	0.28(3)	0.77(5)
Sn	0.0	0.17811	1/4	0.28	0.23
O	0.2758(9)	0.3938(7)	0.420(1)	0.3(1)	1.00

TABLE 3
Anisotropic Displacement Values U_{ij} for $Hf_{0.75}Sn_{0.75}O_2$

Atom	U_{11}	U_{22}	U_{33}	U_{12}	U_{13}	U_{23}
Hf/Sn	0.0035(3)	0.0038(3)	0.0035(4)	0.0	−0.0003(1)	0.0
O	0.005(2)	0.003(1)	0.003(1)	−0.006(2)	−0.007(2)	0.003(2)

TABLE 4
Interatomic Distances Less Than 3.5 Å in $Hf_{0.75}Sn_{0.25}O_2$

Hf–O	2.023(4)	× 2	Hf–Hf	3.3002(6)	× 2
	2.075(4)	× 2			
	2.144(4)	× 2	O–O	2.629(7)	× 1
	3.271(5)	× 2		2.81(1)	× 1
				2.8604(9)	× 2
O–Hf	2.023(4)	× 1		2.870(3)	× 2
	2.075(4)	× 1		3.048(5)	× 2
	2.144(4)	× 1		3.058(9)	× 1
	3.271(5)	× 1		3.085(4)	× 2
				3.21(1)	× 1

TABLE 5
Interatomic Angles within MO_6 Octahedron

O1–*M*–O5	77.1(2)	O2–*M*–O3	96.1(9)
O2–*M*–O6	77.1(2)	O1–*M*–O3	97.7(1)
O5–*M*–O6	81.8(3)	O2–*M*–O4	97.7(1)
O1–*M*–O6	85.7(1)	O3–*M*–O4	105.2(9)
O2–*M*–O5	85.7(1)	O1–*M*–O2	157.2(2)
O3–*M*–O6	86.7(1)	O3–*M*–O5	167.6(2)
O4–*M*–O5	86.7(1)	O4–*M*–O6	167.6(2)
O1–*M*–O4	96.1(9)		

in Table 1. The structure solution and refinement were performed using the SHELXS and TEXSAN software programs (19). Microprobe analysis was done on a Cameca XS50 4-spectometer electron microprobe by wavelength dispersive analysis. Dilatometer data were collected on a Netzsch Thermal Analysis System from room temperature to 800°C with a heating rate of 5°C/min. Calibration and correction from a sapphire standard were applied.

The dielectric constant (K) and the loss factor (tan δ) were measured on a sintered pellet at various frequencies (10^3 to 10^7 Hz) from room temperature to 300°C by the two-terminal method using Hewlett–Packard LCR 4284A and 4285A bridges. The measured dielectric constants were corrected for edge and porosity effects.

RESULTS

The needle-shaped crystals in the two-phase mixture were found to have a tetragonal unit cell with lattice parameters a = 4.776(1) Å and c = 3.2047(6) Å. The X-ray diffraction pattern of the powder matched that for the rutile-type structure of SnO_2 but with a shift in peak positions corresponding to increased lattice parameters resulting from substitution of Sn by Hf (cf. a = 4.737 Å and c = 3.185 Å for SnO_2). Microprobe analysis of a single large crystal of this phase indicated the extent of Hf substitution in $Sn_{1-x}Hf_xO_2$ was in the range $0.36 \pm 0.02 < x < 0.45 \pm 0.02$.

The remaining peaks in the powder diffraction pattern could be indexed according to the α-PbO_2-type structure, with lattice parameters a = 4.8679(8) Å, b = 5.707(2) Å, and c = 5.2098(6) Å. A single-phase sample was prepared with lattice parameters a = 4.8704(4) Å, b = 5.7052(8) Å,

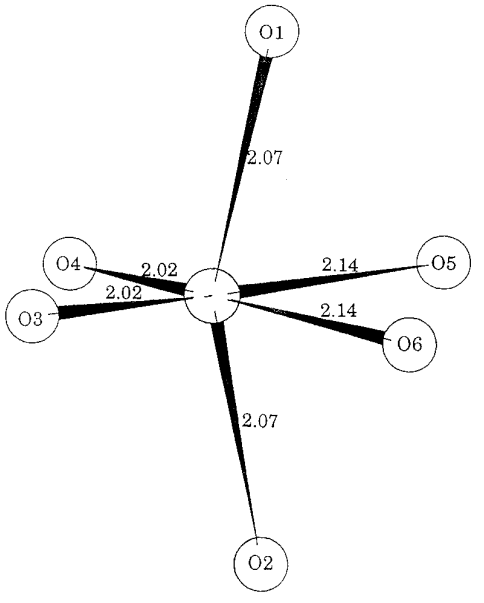

FIG. 2. Metal–oxygen bond lengths in a distorted octahedron.

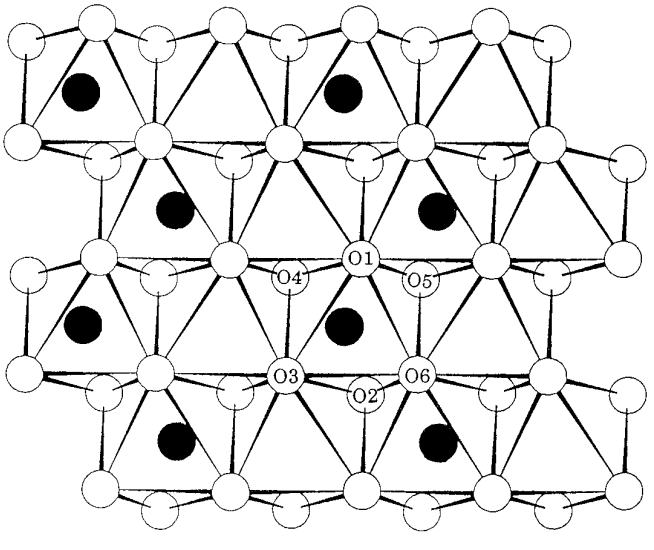

FIG. 1. α-PbO_2 type structure. Numbering of oxygen atoms is the same for Figs. 1–3.

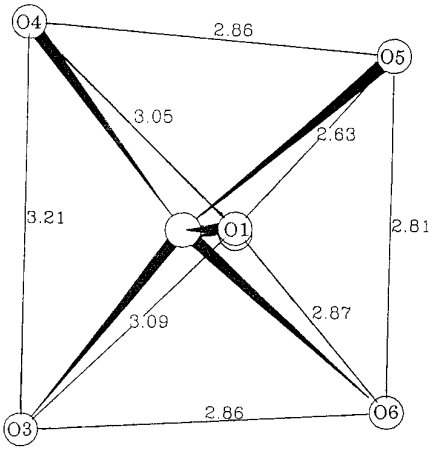

FIG. 3. Oxygen–oxygen bond lengths around a metal-centered octahedron.

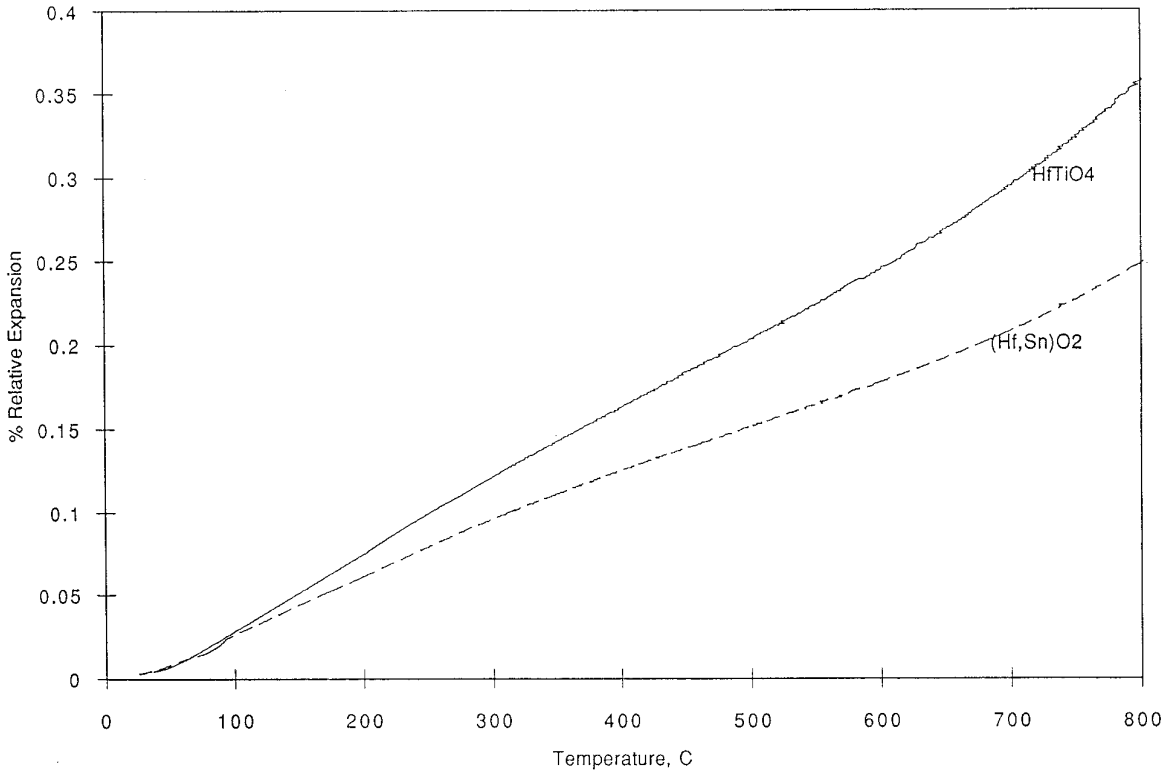

FIG. 4. Linear thermal expansion of $HfTiO_4$ and $Hf_{0.75}Sn_{0.25}O_2$.

and $c = 5.2102(4)$ Å. There was no indication of a superstructure in any of these samples. The single crystal data were collected on a unit cell determined by high-angle cell refinement with lattice parameters $a = 4.861(1)$ Å, $b = 5.699(1)$ Å, and $c = 5.204(1)$ Å. Refinement of mixed occupancy on the metal site gave a metal content of $Hf_{0.77}Sn_{0.23}O_2$. Microprobe analysis on five crystals from the same synthesis suggests a slightly higher Sn content of 0.29 ± 0.01. Thus, unlike (Hf, Ti)O_2, which has a broad range of homogeneity, (Hf, Sn)O_2 has a narrow range of homogeneity at approximately $Hf_{0.75}Sn_{0.25}O_2$. Details of atomic parameters from the single crystal refinement are listed in Tables 2 and 3.

Interatomic bond distances and angles are listed in Tables 4 and 5. The numbering of the oxygen atoms in Table 5 corresponds to the numbering in Figs. 2 and 3. Figure 1 shows the zigzag chains of metal atoms in octahedral sites of distorted close-packed layers of oxygen atoms. Readily apparent is the shift in metal atom position away from the octahedral center, increasing the distance between metal atoms. Note that with the shift of metal atom position away from the shared octahedral edges, these edges form the shortest O–O distance (2.63 Å). Figure 2 shows the metal–oxygen distances, and Fig. 3 shows oxygen–oxygen distances within a single octahedron.

The thermal expansion of $HfTiO_4$ has been previously reported (14–16). The measurement was repeated here for direct comparison with $Hf_{0.75}Sn_{0.25}O_2$. The samples each show a higher rate of expansion from room temperature to 200°C than from 200 to 800°C. This seems to be present in the published plots as well. Plots of relative expansion for $HfTiO_4$ and $Hf_{0.75}Sn_{0.25}O_2$ are given in Fig. 4. Our linear thermal expansion data for $HfTiO_4$ are identical to those reported by Ruh *et al.* for a 50% HfO_2–50% TiO_2 composition (15), which is lower than that reported by Bayer *et al.* (17). We measure $\alpha_{30-200} = 5.0 \times 10^{-6}°C^{-1}$ and $\alpha_{200-800} = 4.3 \times 10^{-6}°C^{-1}$. The thermal expansion of $Hf_{0.75}Sn_{0.25}O_2$ is lower than that of $HfTiO_4$. For $Hf_{0.75}Sn_{0.25}O_2$, $\alpha_{30-200} = 5.0 \times 10^{-6}°C^{-1}$, and $\alpha_{200-800} = 3.4 \times 10^{-6}°C^{-1}$. This is lower expansion than reported for any Zr/Ti/Sn/O compositions, but not as low as reported for some Hf-rich (Hf, Ti)O_2 phases.

The dielectric data for $Hf_{0.75}Sn_{0.25}O_2$ are shown in Fig. 5. As found for other members of the α-PbO_2 family, the dielectric loss is very low and the dielectric constant varies little with frequency or temperature. However, the dielectric constant is lower than observed for the α-PbO_2-type phases which contain Ti.

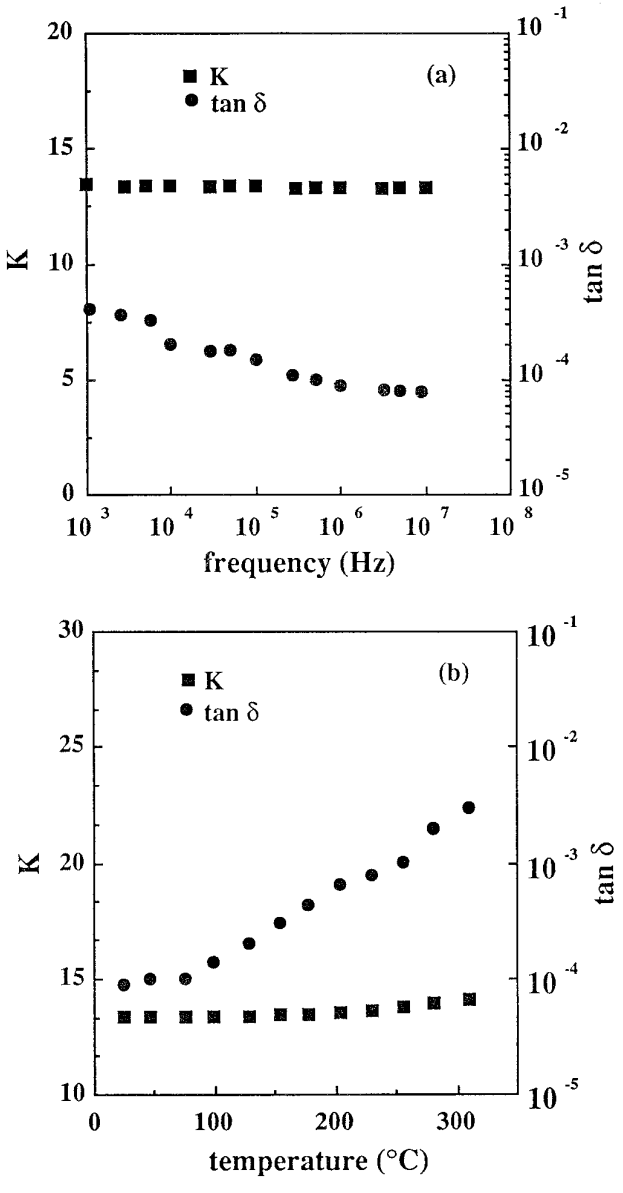

FIG. 5. (a) Variation of $Hf_{0.75}Sn_{0.25}O_2$ dielectric constant with frequency (Hz); (b) variation of $Hf_{0.75}Sn_{0.25}O_2$ dielectric constant at 1 Mhz with temperature.

TABLE 6
Structural Comparison of α-PbO_2-Type Structures

	$ZrTiO_4$	$ZrTi_{0.5}Sn_{0.5}O_4$	$Hf_{1.5}Sn_{0.5}O_4$	$HfTiO_4$
c/b	0.918	0.912	0.913	0.904
Volume, Å^3	131.7	137.5	144.2	135.4
d(*M*–*M*), Å	3.352	3.312	3.300	3.270
O–*M*–O angle	74–111	76–107	77–105	78–108

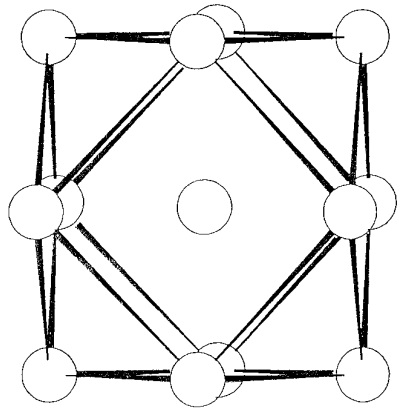

FIG. 6. The α-PbO_2 structure showing only the Pb atoms which are in an approximate cubic close-packed arrangement.

DISCUSSION

The single-crystal structural determinations of $ZrTiO_4$, $ZrTi_{0.5}Sn_{0.5}O_4$, $HfTiO_4$, and now $Hf_{1.5}Sn_{0.5}O_4$ establish that they all crystallize in the α-PbO_2-type structure (12, 18, 19). The structures of the Zr-containing compounds are more distorted than the structures of the Hf compounds, as can be seen by comparison of the values in Table 6. The *c/b* ratio for the unit cells would equal 0.866 for an ideal hexagonal close-packed arrangement of oxygen atoms. The deviation from ideality is greater for $ZrTiO_4$ than for $HfTiO_4$. Another way of comparing this distortion is noting the increased metal–metal distance through the edge-sharing octahedra. The metal–metal distances are greater for the Zr compounds even though the unit cell volumes are smaller. The angles in the metal-centered octahedron which would be 90° in an ideal octahedron show the highest deviations for $ZrTiO_4$.

Both the rutile and α-PbO_2 structures are based on a hexagonally closed-packed arrangement of oxygen anions with cations occupying half of the octahedral sites. However, the high-symmetry tetragonal rutile structure has only one variable positional parameter whereas the orthorhombic α-PbO_2 structure has four variable positional parameters. These extra parameters in the α-PbO_2 structure allow this structure to be much more accommodating. One aspect of this is that the cation lattice approaches cubic close-packing as shown in Fig. 6. This results in less cation–cation repulsion and a denser structure with a higher Madelung energy.

ACKNOWLEDGMENT

This work was supported by NSF Grant DMR-9308530.

REFERENCES

1. G. Wolfram and H. E. Göbel, *Mater. Res. Bull.* **16,** 1455 (1981).
2. K. Wakino, K. Minai, and H. Tamura, *J. Am. Ceram. Soc.* **67,** 278 (1984).
3. K. Wakino, *in* "Proceedings, 6th IEEE International Symposium on Applications of Ferroelectrics, Lehigh University, Bethlehem, PA, June 8–11, 1986," p. 97.
4. A. E. McHale and R. S. Roth, *J. Am. Ceram. Soc.* **66,** C18 (1983).
5. A. E. McHale and R. S. Roth, *J. Am. Ceram. Soc.* **69,** 827 (1986).
6. R. Kudesia, R. L. Snyder, R. A. Condrate, Sr., and A. E. McHale, *J. Phys. Chem. Solids* **54,** 671 (1993).
7. R. Kudesia, A. E. McHale, R. A. Condrate, Sr., and R. L. Snyder, *J Mater. Sci.* **28,** 5569 (1993).
8. S. Hirano, T. Hayashi, and A. Hattori, *J. Am. Ceram. Soc.* **74,** 1320 (1991).
9. D. B. Rogers, R. D. Shannon, A. W. Sleight, and J. L. Gillson, *Inorg. Chem.* **8,** 841 (1969).
10. Muller and Roy, *in* "Crystal Chemistry of Non-Metallic Materials," Vol. 4, Springer-Verlag, New York, 1974.
11. J. Stöcker and R. Collongues *C. R. Acad. Sci.* **245,** 431 (1957).
12. R. E. Newnham, *J. Am. Ceram. Soc.* **50,** 216 (1967).
13. P. Bordet, A. McHale, A. Santoro, and R. S. Roth, *J. Solid State Chem.* **64,** 30 (1986).
14. R. W. Lynch and B. Morosin, *J. Am. Ceram. Soc.* **55,** 409 (1972).
15. R. Ruh, G. W. Hollenberg, E. G. Charles, and V. A. Patel, *J. Am. Ceram. Soc.* **59,** 495 (1976).
16. H. Ikawa, A. Iwai, K. Hiruta, H. Shimojima, K. Urabe, and S. Udagawa, *J. Am. Ceram. Soc.* **71,** 120 (1988).
17. G. Bayer, M. Hofmann, and L. J. Gauckler, *J. Am. Ceram. Soc.* **74,** 2205 (1991).
18. A. W. Sleight, *Endeavour* **19,** 64 (1995).
19. (a) G. M. Sheldrick, *in* "Crystallographic Computing 3" (G. M. Sheldrick, C. Krüger, R. Goddard, Eds.), p. 175, Oxford Univ. Press, Oxford, 1985. (b) "TEXSAN: Single Crystal Structure Analysis Software, Version 5.0 (1989)." Molecular Structures Corporation, The Woodlands, 1989.
20. A. Harari, J.-P. Bocquet, M. Huber, R. Collongues, *C. R. Acad. Sci. Paris Ser. C* **267,** 1316 (1968).
21. A. Siggel and M. Jansen, *Z Anorg. Allg. Chem.* **582,** 93 (1990).